Formation and tuning of moiré excitons in large-twist angle WS2/MoSe2 heterobilayers

Long Zhang
Physics Department, University of Michigan, 450 Church Street, Ann Arbor, MI 48109-2122, USA
https://orcid.org/0000-0003-0988-6736

Zhe Zhang
Physics Department, University of Michigan, 450 Church Street, Ann Arbor, MI 48109-2122, USA

Fengcheng Wu
Condensed Matter Theory Center and Joint Quantum Institute, Department of Physics, University of Maryland, College Park, Maryland 20742, USA https://orcid.org/0000-0002-1185-0073

Danqing Wang
Physics Department, University of Michigan, 450 Church Street, Ann Arbor, MI 48109-2122, USA

Rahul Gogna
Applied Physics Program, University of Michigan, 450 Church Street, Ann Arbor, MI 48109-1040, USA

Shaocong Hou
Department of Electrical Engineering and Computer Science, University of Michigan, 450 Church Street, Ann Arbor, MI 48109-1040, USA

Kenji Watanabe
National Institute for Materials Science, Tsukuba, Ibaraki, 305-0044 Japan https://orcid.org/0000-0003-3701-8119

Takashi Taniguchi
National Institute for Materials Science, Tsukuba, Ibaraki, 305-0044 Japan

Krishnamurthy Kulkarni
Department of Electrical Engineering and Computer Science, University of Michigan, 450 Church Street, Ann Arbor, MI 48109-1040, USA

Thomas Kuo
Physics Department, University of Michigan, 450 Church Street, Ann Arbor, MI 48109-2122, USA

Stephen Forrest
Physics Department, University of Michigan, 450 Church Street, Ann Arbor, MI 48109-2122, USA

Hui Deng (dengh@umich.edu)
Physics Department, University of Michigan, 450 Church Street, Ann Arbor, MI 48109-2122, USA
https://orcid.org/0000-0003-0629-3230

Article

Keywords: moire lattices, van der Waals bilayers, twist angles

Posted Date: July 1st, 2020

DOI: https://doi.org/10.21203/rs.3.rs-37553/v1

Version of Record: A version of this preprint was published at Nature Communications on November 18th, 2020. See the published version at https://doi.org/10.1038/s41467-020-19466-6.

Formation and tuning of moiré excitons in large-twist angle $WS_2/MoSe_2$ heterobilayers

Long Zhang[1], Zhe Zhang[1,2], Fengcheng Wu[3], Danqing Wang[1], Rahul Gogna[4], Shaocong Hou[5], Kenji Watanabe[6], Takashi Taniguchi[6], Krishnamurthy Kulkarni[5], Thomas Kuo[1], Stephen R. Forrest[1,5] and Hui Deng[1,4*]

[1] *Physics Department, University of Michigan, 450 Church Street, Ann Arbor, MI 48109-2122, USA*

[2] *State Key Laboratory of Surface Physics, Department of Physics, Fudan University, Shanghai 200433,China*

[3] *Condensed Matter Theory Center and Joint Quantum Institute, Department of Physics, University of Maryland, College Park, Maryland 20742, USA*

[4] *Applied Physics Program, University of Michigan, 450 Church Street, Ann Arbor, MI 48109-1040, USA*

[5] *Department of Electrical Engineering and Computer Science, University of Michigan, 450 Church Street, Ann Arbor, MI 48109-1040, USA and*

[6] *National Institute for Materials Science, Tsukuba, Ibaraki, 305-0044 Japan*

Abstract

Moiré lattices formed in twisted van der Waals bilayers provide a unique, tunable platform to realize coupled electron or exciton lattices unavailable before. While twist angle between the bilayer has been shown to be a critical parameter in engineering the moiré potential and enabling novel phenomena in electronic moiré systems, studies of moiré excitons so far have focused on closely angularly-aligned heterobilayers. The twist-angle degree of freedom has been largely considered detrimental to the observation of moiré excitons. Here we report robust moiré excitons in bilayers of even large twist angles formed due to Umklapp scattering by the moiré reciprocal lattice vectors, and we furthermore demonstrate twist-angle tuning of the properties of the moiré excitons as a result of varying moiré reciprocal lattice periods. We develop an intuitive analytical model to explain our results, and, from the twist-angle dependence, obtain the effective mass of the interlayer excitons and the electron inter-layer tunneling strength, which are difficult to measure experimentally otherwise. These findings pave the way for understanding and engineering rich moiré -lattice induced phenomena in angle-twisted semiconductor van der Waals semiconductor heterostructures.

Atomically thin heterostructures created by stacking van der Waals materials mark a new frontier in condensed matter physics [1–3]. When two monolayer crystals of the same lattice symmetries overlay on each other, a moiré superlattice may form due to a small mismatch in their lattice constants or angular alignment [4, 5]. The latter – the twist angle between the two layers – provides a powerful tuning knob of the electronic properties of the heterostructure. Seminal results have been obtained in twisted bilayer graphene, where superconducting and correlated insulating states are created by fine control of the twist angle [6–9]. In semiconductors, such as transition metal dichalcogenides (TMDC) heterobilayers, the moiré lattice has a period on the length scale of an exciton, thereby providing a unique opportunity to create coupled exciton lattices hitherto unavailable in any other systems. A wide variety of phenomena, tunable with the twist angle, may become possible, ranging from single quantum-dot arrays and topological bands to strongly correlated states [10–14].

To search for the effects of moiré lattices on excitons, split exciton states have been reported in TMDC bilayers with very small twist angles, showing localization of exciton states likely in moiré super-cells [15–18]. However, increasing the twist angle has led to suppression of measurable

features of moiré excitons. In WS_2 /$MoSe_2$ heterobilayers, it was suggested that the resonant interlayer hybridization amplifies the moiré superlattice effects on the electronic structure [19]; yet only a single resonance was resolved as the twist angle deviates significantly from 0° or 60° [18]. Existence of moiré superlattice for exciton in large-twist-angle bilayers and nontrivial effects of the twist-angle on excitons remain largely unexplored in experiments.

In this work, we show moiré excitons in heterobilayer of a wide range of twist angles and demonstrate tuning of their properties by the moiré lattice of varying periods. Utilizing the inter- and intra-layer hybrid excitons in WS_2 /$MoSe_2$ bilayers, we reveal the formation of moiré reciprocal lattices with Brillouin zones of different sizes at different twist angles. We furthermore show how the moiré reciprocal lattices drastically change the properties of the moiré excitons, such as their resonance energies, oscillator strengths, and inter-/intra-layer mixing. The twist-angle dependence of the moiré exciton states are well-explained by an analytical theory model based on band-folding in the moiré lattice, which also consistently explain the dependence on the spin-orbit splitting of the conduction band, valley selection rules, atomic stacking orders and the lattice symmetries. Comparing the experimental results with the model, we obtain the effective mass of the interlayer excitons, the inter-layer electron tunneling strength. These results showcase moiré -lattice tuning as a new route to uncover and tune fundamental properties of heterobilayer systems, and open the door to studies of moiré exciton physics in twisted bilayers beyond graphene.

RESULTS

The devices used in this work are WS_2 /$MoSe_2$ heterobilayers with different twist angles θ, capped by few-layer hexagonal boron nitride (hBN). Details of sample fabrication and calibration of θ have been described elsewhere [20, 21] and provided in the Method section. Fig. 1a shows the optical microscope image of a heterobilayer, where the sharp edges of two monolayers are aligned. The twist angle is $\theta = 59.8° \pm 0.3°$, determined optically using polarization-dependent second-harmonic-generation measurements [20, 21] (See Supplemental Material Fig.S1 and Fig.S2 for details).

Identification and analysis of inter- and intra-layer hybrid excitons

We first characterize exciton hybridization in closely aligned hetero-bilayers, with a twist angle $\theta \sim 0°$ or 60°. In such bilayers, the Brillouin zones of the two layers closely overlap in momentum space to form nearly direct bandgaps for both the inter- and intra-layer transitions (top panels of Fig. 1b). At the same time, the hole band offset is large but the conduction band offset is small between WS_2 and $MoSe_2$ (middle panels of Fig. 1b). Therefore inter-layer electron tunneling is expected between states of the same spin and valley, which leads to hybridization between the corresponding intra- and inter-layer exciton transitions that share the same hole state (bottom panels of Fig. 1b).

Making use of the large difference in oscillator strength between spatially direct and indirect excitons, we can identify the formation of hybrid states via the reflectance contrast (RC) spectra: $RC = \frac{R_{sample}-R_{sub}}{R_{sub}}$, where R_{sample} and R_{sub} are reflection spectrum taken from sample and substrate respectively (See Supplemental Material Fig.S3). The interlayer exciton has an oscillator strength two to three orders of magnitude weaker than that of the intra-layer exciton, due to separation of the electron and hole wavefunction[22, 23], so it is typically too weak to be measurable in absorption or RC spectroscopy where the noise level is typically 1% or higher (Supplemental Material Fig.S4). However, when interlayer excitons hybridize with intra-layer ones via electron or hole tunneling, the hybrid states acquire an oscillator strength through the intra-layer exciton component. Therefore, we can identify the hybrid excitons via their spectral weight in the absorption spectra of the heterobilayer.

As shown in Fig. 1c, the $MoSe_2$ monolayer region of the device (as marked on Fig. 1a) shows a strong intralayer $MoSe_2$ A exciton resonance near 1.65 eV, while the WS_2 monolayer has no exciton resonances nearby. In the bilayer, stacking of the WS_2 layer is expected to lead to a red shift of $MoSe_2$ A exciton resonance[18] while also introduce an interlayer exciton transition, between an electron in WS_2 and a hole in $MoSe_2$. The interlayer exciton has a negligible oscillator strength and should not be observable in RC. However, two clearly-resolved resonances appear in our bilayer, both with significant spectral weight (top two spectra in Fig. 1c). The same two resonances are also measured in photoluminescence (See Supplemental Material Fig.S5). We therefore identify them as the inter- and intra-layer hybrid states, the lower (LHX) and upper hybrid excitons (UHX). Both LHX and UHX inherit an oscillator strength from their intra-layer component [18], with the

ratio f_{LHX}/f_{UHX} controlled by their intra-layer exciton fractions, which in turn is controlled by the energy detuning $\delta = E_{IX} - E_X$ between the uncoupled inter-layer (E_{IX}) and intra-layer (E_X) resonances. Therefore f_{LHX}/f_{UHX} greater or less than one corresponds to positive or negative detuning δ. There are multiple pairs of intra- and inter-layer excitons that can hybridize. We focus on the transition region of $MoSe_2$ A exciton first and label these states as MoA excitons, of which the hole is always in the highest $MoSe_2$ valence band. Other pairs will be analyzed later.

As clearly seen in Fig. 1c, in the R-stacking bilayers ($\theta = 2.1°$), $f_{LHX}/f_{UHX} > 1$, suggesting the uncoupled interlayer state lies above the intralayer one, or $\delta_R > 0$. In contrast, in the H-stacking bilayer ($\theta = 59.8°$), $f_{LHX}/f_{UHX} < 1$, suggesting $\delta_H < 0$. These results are consistent with the spin selection rules of the excitonic transitions illustrated in Fig. 1b [24] ,and the difference $\delta_R - \delta_H$ corresponds to the spin-orbit splitting of WS_2 conduction band (Fig. 1b).

To analyze the results quantitatively, we first obtain the energies, E_{LHX} and E_{UHX}, and oscillator strengths of the hybrid states by fitting the RC spectra using the transfer matrix method, where the hybrid excitons are modeled as Lorentz oscillators (See Supplemental Material Fig.S3) [24, 25]. The fitted spectrum agrees well with the data, as shown in Fig. 1c. Describing the hybrid modes with the coupled oscillator model, we have $E_{LHX} - E_{UHX} = -\sqrt{4J^2 + \delta^2}$, and $\frac{f_{LHX}}{f_{UHX}} = \frac{\sqrt{\delta^2+4J^2}+\delta}{\sqrt{\delta^2+4J^2}-\delta}$ (See Supplemental Materials Sec.I for details). Thereby using the fitted $E_{LHX,UHX}$ and $f_{LHX,UHX}$, we can obtain δ and J. As summarized in Fig. 1d, we obtain $J \sim 20$ meV for both R- and H-stacking and $\delta_R - \delta_H = 25.9 \pm 0.5$ meV [26], consistent with the spin-orbit splitting of WS_2 [27], confirming the hybrid states are formed by spin-conserved inter-layer electron tunneling.

Twist-angle dependence of moiré -lattice induced hybrid excitons

To study tuning of the hybrid excitons by the moiré lattice, we perform the same measurements and analysis as discussed above on 30 samples with different twist angles, and obtain how the exciton energies, oscillator strengths and inter-layer tunneling vary with the changing moiré lattice. We define $\theta_0 < 30°$ as the angular deviation from aligned bilayers of R- or H-stacking. $\theta_0 = |\theta|$ for R-stacking and $\theta_0 = |60° - \theta|$ for H-stacking.

As shown in Fig. 2a, the MoA hybrid exciton doublets are clearly resolved for θ_0 up to 6°, which would correspond to a tuning of the moiré lattice constant by nearly three-fold [28]. The spectral weights of the doublets evolve continuously with the twist angle, reflecting continuous increase of

f_{LHX}/f_{UHX} and δ with θ_0 (middle panel of Fig. 2c). At the same time, the inter-layer coupling J decreases continuously (bottom panel of Fig. 2c). These observations show clearly moiré lattice induce hybridization and tuning of intra-layer and inter-layer excitons, as we explain below.

We illustrate in Fig. 2b the MoA exciton bands at different twist angles, corresponding to the six samples shown in Fig. 2a. The intra-layer $MoSe_2$ A exciton transition (red band) remains direct, with the band minimum at zero center-of-mass momentum $\boldsymbol{q}_X \sim 0$, irrespective of the twist angle. It is close in energy with the inter-layer exciton formed by a hole from the same $MoSe_2$ valence band but an electron from a WS_2 conduction band. This inter-layer exciton band has the band minimum also at zero center of mass momentum: $\boldsymbol{q}_{IX} \sim 0$, when $\theta \sim 0^\circ$ (θ_1 in Fig. 2a-b) or 60° (θ_6 in Fig. 2a-b), neglecting the small lattice constant mismatch.

As the two lattices rotate relative to each other by θ (θ_2 to θ_5 in Fig. 2a-b), the Brillouin zones of $MoSe_2$ and WS_2 also rotate by θ. The inter-layer exciton band minimum shifts away from the intra-layer exciton band minimum by momentum $\boldsymbol{K}_W - \boldsymbol{K}_M$ for R stacking, where $\boldsymbol{K}_M$ and $\boldsymbol{K}_W$ are respectively the Brillouin zone corners for $MoSe_2$ and WS_2 layers. Due to this momentum mismatch, hybridization between intra-layer $MoSe_2$ A excitons and the interlayer state at the band minimum is not allowed.

However, interlayer electron tunneling in the moiré lattice can lead to the formation of new moiré miniband states to hybridize with the optically bright intralayer excitons. As illustrated in Fig. 2b and Fig. 3c, three interlayer excitons $|\boldsymbol{q}_i\rangle_{\mathrm{IX}}$ overlap with the optically bright intralayer exciton, where the center of mass momentum $\boldsymbol{q}_i$, measured relative to the band minimum of interlayer exciton, correspond to $\boldsymbol{q}_1 = \boldsymbol{K}_M - \boldsymbol{K}_W$ for R-stacking, with $\boldsymbol{q}_{2,3}$ connected to $\boldsymbol{q_1}$ by $2\pi/3$ and $4\pi/3$ rotations, respectively, via moiré reciprocal lattice vectors. These three inter-layer states are offset from their band minimum by the kinetic energy $\hbar^2 q_i^2/(2M_{\mathrm{IX}})$, for $i = 1, 2, 3$ and M_{IX} the total mass of inter-layer exciton. These three states can couple due to the moiré lattice and therefore, superpose to form moiré minband states, of which one interlayer exciton state shares the same angular momentum as the intra-layer $MoSe_2$ A exciton at $q_X \sim 0$, giving rise to the hybrid doublet we observe in angularly misaligned bilayers (See Supplemental Material Sec.II).

When θ deviates more from 0° or 60°, the interlayer exciton formed in the moiré lattice continuously blueshifts because of the increasing kinetic energy, which explains the measured continuous blueshift of the LHX and UHX resonances, and the continuous increase of the spectral weight of LHX compared to UHX.

Theoretical analysis of moiré -lattice induced hybrid excitons

To analyze our results more quantitatively, we develop an analytical microscopic theory based on the above understanding (See Supplemental Material Sec.II for details). Comparing it with the measured twist-angle dependence of the hybrid states, we obtain the key band parameters of the bilayer, including the interlayer exciton effective mass and interlayer coupling strength.

We first compare the measured detuning δ with θ_0 and the interlayer exciton kinetic energy. As discussed above, δ is given by:

$$\delta(\theta_0) = \delta_0 + \frac{\hbar^2 \boldsymbol{q}_1^2}{2M_{\mathrm{IX}}}, \tag{1}$$

where δ_0 is the detuning at $\theta = 0^\circ$ or 60° for bilayers close to R- and H-stacking, respectively. $\boldsymbol{q}_1$ is equal to $4\pi/(3a_M)$, and a_M is the moiré period approximated by $a_0/\sqrt{\theta_0^2+\epsilon^2}$, for a_0 the monolayer lattice constant and ϵ the lattice constant mismatch $|a_0 - a_0'|/a_0$ between the two layers. Equation. (1) shows that δ increases quadratically with θ_0. As θ_0 increases from $0^\circ$to 6°, a_M changes by nearly three fold, and $\delta - \delta_0$ changes by seven-fold [28]. Fitting the measured δ vs. θ_0 with Equation. (1), we find the inter-layer exciton total mass M_{IX} to be $(6.9 \pm 3.2)m_0$ and $(1.41 \pm 0.28)m_0$ for R- and H-stacking heterobilayers, respectively, for m_0 the electron free mass.

From our microscopic theory, we can also estimate the conduction-band interlayer tunneling parameter w from the coupling strength J through the relation

$$J = \frac{\sqrt{3}w}{\mathcal{A}} \sum_{\boldsymbol{k}} \phi^*_{\boldsymbol{k}+\frac{m_{h,IX}}{M_{\mathrm{IX}}}\boldsymbol{q}_1} \psi_{\boldsymbol{k}}, \tag{2}$$

where $\phi_{\boldsymbol{k}}$ and $\psi_{\boldsymbol{k}}$ are respectively the relative-motion wave function for interlayer and intralayer excitons with the normalizations $(1/\mathcal{A})\sum_{\boldsymbol{k}} |\psi_{\boldsymbol{k}}|^2 = 1$ and $(1/\mathcal{A})\sum_{\boldsymbol{k}} |\phi_{\boldsymbol{k}}|^2 = 1$. Here $\mathcal{A}$ is the system area and $m_{h,IX}$ is the hole mass for the interlayer exciton. Because of the momentum shift $(m_{h,IX}/M_{\mathrm{IX}})\boldsymbol{q}_1$ in the integral of Eq. (2), J decreases with increasing θ_0, which agrees with the experimentally observed angle dependence of J. At small θ_0, J can be approximated by $\sqrt{3}w$. Using our experimentally measured value of J at $\theta_0 \sim 0$, we estimate the interlayer tunneling w to be about 14 meV for both R- and H-stacking bilayers.

When the twist angle θ_0 is greater than 6°, the hybrid exciton doublets become hard to be resolved, likely because there is a large blue detuning and the UHX has a vanishing oscillator strength (See Supplemental material Fig. S6).

Moiré excitons in commensurate moiré lattices at twist angles near 21.8° and 38.2°

Remarkably, pronounced and well-resolved doublets re-appear in hetero-bilayers with $\theta = 20.1^\circ \pm 0.3$ and $40.3^\circ \pm 0.3$, as shown in Fig. 3. In the bilayer with 20.1° twist angle, the LHX has a smaller spectral weight than UHX has, corresponding to a negative detuning ($\delta = -5.6$ meV), which is similar to H-stacking bilayers formed at $\theta \sim 60^\circ$. In contrast, in the bilayer with 40.3° twist angle, the LHX has a larger spectral weight than UHX has, corresponding to a positive detuning ($\delta = 11.8$ meV), which is similar to R-stacking bilayers formed at $\theta \sim 0^\circ$. In both devices, the coupling strength $J \sim 8$ meV is weaker than but of the same order of magnitude as aligned bilayers with θ close to 0° or 60°.

The revival of hybrid excitons in these two bilayers can be understood as a direct result of interlayer tunneling induced by a moiré lattice that is nearly commensurate with the monolayer lattices. The two twist angles are close to the commensurate angles 21.8° and 38.2°, respectively. At the commensurate angles, the moiré reciprocal lattice constant is $1/\sqrt{7}$ of the monolayer reciprocal lattice constant, and corners of the Brillouin zones of the two monolayers become connected by moiré reciprocal lattice vectors, as illustrated in Figs. 3d and e. The $MoSe_2$ and WS_2 band minima overlap again in the moiré reciprocal lattice, allowing strong nearly-resonant tunneling between the intra- and inter-layer states. Specifically, when $\theta \approx 21.8^\circ$, K-valley of $MoSe_2$ and K'-valley of WS_2 are connected by moiré reciprocal lattice vectors and are folded into equivalent momentum in the moiré Brillouin zone (Fig. 3d). The corresponding hybridized excitons have the same valley configuration as those in bilayers with $\theta \sim 60^\circ$, which is consistent with the observed negative detuning. When $\theta \approx 38.2^\circ$, K-valley of $MoSe_2$ and K-valley of WS_2 are folded into equivalent momentum in the moiré Brillouin zone (Fig. 3e), and the corresponding hybridized excitons have the same valley configuration as those in bilayers with $\theta \sim 0^\circ$, consistent with the observed positive detuning. Moreover, since interlayer tunneling only needs one Umklapp scattering by a moiré reciprocal lattice vector, the tunneling strength remains of the same order of magnitude as in angularly aligned bilayers. Therefore, the strong revival of the hybrid excitons and their similarities with the angularly-aligned bilayers show again the critical role of moiré lattice in interlayer tunneling.

Moiré excitons formed with different intra-layer excitons

In the above discussion, we have focused on hybrid states formed with the $MoSe_2$ A excitons, which feature large spectral weight, relatively narrow linewidths, and well-resolved doublets at small detunings. Hybrid states can also form with higher-energy bands, including the $MoSe_2$ B, WS_2 A and WS_2 B excitons. The B excitons have broader linewidths than the A excitons; as a result the doublets are not well resolved. The WS_2 A excitons have a broader linewidth than $MoSe_2$ A excitons and generally a larger detuning. We observe well-resolved WA doublets only in bilayers with $\theta \sim 0°$, corresponding to hybrid excitons formed by a hole in the WS_2 valence band and an electron tunneling between the $MoSe_2$ and WS_2 conduction bands (Fig. 4).

It is interesting to compare the detuning for MoA and WA states for $\theta \sim 0°$, which we label as δ_{MoA} and δ_{WA}, respectively. As shown in the schematic electronic band diagram in Fig. 4a, neglecting exciton binding energies, the detuning of the inter-layer transition from the intra-layer one is the same magnitude but opposite signs between the MoA and WA states. The sum of the two detuning should be zero. However, this is different from our observation that both the LHX states have larger spectral weight for both MoA and WA states. This can be understood as due to the weaker binding energy of interlayer excitons compared to intra-layer ones, resulting from electron-hole separation. The difference in intra- and inter-layer exciton binding energies, $\Delta E_B^R = E_{BX} - E_{BIX}$, adds to both δ_{MoA} and δ_{WA}. Assuming ΔE_B^R is approximately the same for the MoA and WA state, the sum of δ_{MoA} and δ_{WA} becomes twice of ΔE_B, or, $\Delta E_B^R = 1/2(\delta_{MoA} + \delta_{WA})$. From our measurements of MoA and WA states in bilayers with $\theta < 1°$, we estimate ΔE_B^R of 10 to 16 meV (Fig. 4b). The value is significantly lower than predictions based on first principle calculations when interlayer tunneling is neglected [29, 30].

DISCUSSION

Our results demonstrate hybrid states formed between momentum-direct, moiré -induced inter-layer and intra-layer excitons in twisted WS_2 /$MoSe_2$ bilayers. Deviation of the twist angle from 0° or 60° not only does not suppress moiré excitons but provides a sensitive tuning knob of the moiré excitons' properties. Persistence of the moiré excitons, or, the moiré lattice, is clearly manifested in the inter-layer tunneling strength, which remains within the same order of magnitude over

the measured range of twist angles. This is possible because momentum conservation between the twisted layers is restored by the moiré lattice, or Umklapp scattering by the moiré reciprocal lattice vector. Remarkably, while large detuning between the inter-layer and intra-layer states suppresses hybridization over a range of angles, pronounced hybrid moiré excitons due to strong inter-layer tunneling reappears near twist angles of 21.8° and 38.2°. At these angles, moiré -lattices are formed commensurate with the monolayer lattices, bringing angularly shifted valleys of the two monolayers into equivalent momentum in the same moiré Brillouin zone, thereby enabling strong inter-layer tunneling [31]. The resulting hybrid exciton states resemble the features in hetero-bilayers with $\theta = 60°$ and 0°, respectively. These results are direct manifestations of the discrete translational symmetry of the underlying moiré superlattice, which enables transitions that otherwise would not conserve momentum.

Furthermore, the demonstrated twist-angle tuning of the moiré -lattice provides a route to uncover fundamental properties of heterobilayer systems, and may enable tuning and control of exotic states of matter with novel applications in nanophotonics and quantum information science. Since the hybrid excitons are formed in moiré reciprocal lattices, their properties dependent sensitively on the moiré period, or the twist angle. From the twist-angle dependence, parameters of the bilayer system are obtained, including conduction band splitting of WS_2 induced by spin orbital coupling, effective mass of the interlayer excitons in R- and H-stacking bilayers, and the interlayer electron tunneling strength. These properties are difficult to measure otherwise.

The hybrid excitons inherit large oscillator strengths from the intra-layer component that may allow strong exciton-photon coupling while, at the same time, inherit static dipole moment from the spatially indirect inter-layer component that leads to long-range interactions. Both the oscillator strength and dipole interactions are tuned by the twist angle. The twisted WS_2 /$MoSe_2$ bilayers may provide tunable, nonlinear, exciton and polariton lattice systems for exotic states of matter , such as topological excitons and exciton crystals [10–13, 32–47].

METHODS

Sample fabrication.

Monolayer $MoSe_2$, WS_2 and few layer hexagonal boron nitride (hBN) flakes are obtained by mechanical exfoliation from bulk crystals. A PET stamp was used to pick up the top hBN, WS_2 monolayer, $MoSe_2$ monolayer, and the bottom hBN under microscope. After picking up all the layers, PET stamp was then stamped onto sapphire substrate, and the PET was dissolved in dichloromethane for six hours at room temperature.

Optical measurements.

For low temperature measurements, the sample is kept in a 4 K cryostat (Montana Instrument). The excitation and collection are carried out with a home-built confocal microscope with an objective lens with numerical aperture (NA) of 0.42. For reflection contrast measurement, white light from a tungsten halogen lamp is focused on the sample with a beam size of 10 μm in diameter. The spatial resolution is improved to be 2 μm by using pinhole combined with confocal lenses. The signal is detected using a Princeton Instruments spectrometer with a cooled charge-coupled camera.

Data availability Data are available on request from the authors.

Competing interests The authors declare that they have no competing financial interests.

Author Contributions H.D., L.Z.conceived the experiment. L.Z. and Z.Z fabricated the device and performed the measurements. F.W. performed the modeling and calculations. L.Z. and H.D. performed data analysis. R.G performed tunneling estimation. D.W, S.H, K.K. and T.G assisted the fabrication. K.W. and T.T grew hBN single crystals. H.D. and S.F. supervised the projects. L.Z, F.W. and H.D. wrote the paper with inputs from other authors. All authors discussed the results, data analysis and the paper.

acknowledgments L.Z.,R.G,S.H, S.F.and H.D.acknowledge the support by the Army Research Office under Awards W911NF-17-1-0312. F. W. is supported by Laboratory for Physical Sciences. K.W. and T.T. acknowledge support from the Elemental Strategy Initiative conducted by the MEXT, Japan and the CREST (JPMJCR15F3), JST. S.F. also acknowledges support by the U.S. Department of Energy, Office of Science, Office of Basic Energy Sciences, under Award Number

DE-SC0017971.

* dengh@umich.edu

[1] Geim, A. K. & Grigorieva, I. V. Van der Waals heterostructures. *Nature* **499**, 419–425 (2013).

[2] Novoselov, K. S., Mishchenko, A., Carvalho, A. & Castro Neto, A. H. 2d materials and van der Waals heterostructures. *Science* **353**, aac9439–aac9439 (2016).

[3] Rivera, P. *et al.* Valley-polarized exciton dynamics in a 2d semiconductor heterostructure. *Science* **351**, 688–691 (2016).

[4] Kuwabara, M., Clarke, D. R. & Smith, D. A. Anomalous superperiodicity in scanning tunneling microscope images of graphite. *Applied Physics Letters* **56**, 2396–2398 (1990).

[5] Zhang, C. *et al.* Interlayer couplings, moiré patterns, and $2D$ electronic superlattices in MoS_2/WSe_2 hetero-bilayers. *Science advances* **3**, e1601459 (2017).

[6] Cao, Y. *et al.* Unconventional superconductivity in magic-angle graphene superlattices. *Nature* **556**, 43–50 (2018).

[7] Cao, Y. *et al.* Correlated insulator behaviour at half-filling in magic-angle graphene superlattices. *Nature* **556**, 80–84 (2018).

[8] Chen, G. *et al.* Signatures of tunable superconductivity in a trilayer graphene moiré superlattice. *Nature* **572**, 215–219 (2019).

[9] Chen, G. *et al.* Evidence of a gate-tunable Mott insulator in a trilayer graphene moiré superlattice. *Nature Physics* **15**, 237–241 (2019).

[10] Wu, F., Lovorn, T. & MacDonald, A. H. Topological exciton bands in moiré heterojunctions. *Phys. Rev. Lett.* **118**, 147401 (2017).

[11] Yu, H., Liu, G.-B., Tang, J., Xu, X. & Yao, W. Moiré excitons: From programmable quantum emitter arrays to spin-orbitcoupled artificial lattices. *Science Advances* **3**, e1701696 (2017).

[12] Wu, F., Lovorn, T. & MacDonald, A. H. Theory of optical absorption by interlayer excitons in transition metal dichalcogenide heterobilayers. *Phys. Rev. B* **97**, 035306 (2018).

[13] Wu, F., Lovorn, T., Tutuc, E. & MacDonald, A. Hubbard Model Physics in Transition Metal Dichalcogenide Moiré Bands. *Phys. Rev. Lett.* **121**, 026402 (2018).

[14] Tong, Q. *et al.* Topological mosaics in moiré superlattices of van der Waals heterobilayers. *Nature Physics* **13**, 356–362 (2017).

[15] Jin, C. *et al.* Observation of moiré excitons in WSe_2/WS_2 heterostructure superlattices. *Nature* **567**, 76–80 (2019).

[16] Tran, K. *et al.* Evidence for moiré excitons in van der Waals heterostructures. *Nature* **567**, 71–75 (2019).

[17] Seyler, K. L. *et al.* Signatures of moiré-trapped valley excitons in $MoSe_2/WSe_2$ heterobilayers. *Nature* **567**, 66–70 (2019).

[18] Alexeev, E. M. *et al.* Resonantly hybridized excitons in moiré superlattices in van der Waals heterostructures. *Nature* **567**, 81–86 (2019).

[19] Ruiz-Tijerina, D. A. & Fal'ko, V. I. Interlayer hybridization and moiré superlattice minibands for electrons and excitons in heterobilayers of transition-metal dichalcogenides. *Phys. Rev. B* **99**, 125424 (2019).

[20] Zhang, L. *et al.* Highly valley-polarized singlet and triplet interlayer excitons in van der waals heterostructure. *Phys. Rev. B* **100**, 041402 (2019).

[21] Paik, E. Y. *et al.* Interlayer exciton laser of extended spatial coherence in atomically thin heterostructures. *Nature* **576**, 80–84 (2019).

[22] Ross, J. S. *et al.* Interlayer Exciton Optoelectronics in a 2d Heterostructure pn Junction. *Nano Letters* **17**, 638–643 (2017).

[23] Van der Donck, M. & Peeters, F. M. Interlayer excitons in transition metal dichalcogenide heterostructures. *Phys. Rev. B* **98**, 115104 (2018).

[24] Hsu, W.-T. *et al.* Tailoring excitonic states of van der waals bilayers through stacking configuration, band alignment, and valley spin. *Science Advances* **5**, 12 (2019).

[25] Li, Y. *et al.* Measurement of the optical dielectric function of monolayer transition-metal dichalcogenides: MoS_2, $MoSe_2$, WS_2, and WSe_2. *Phys. Rev. B* **90**, 205422 (2014).

[26] Considering the lattice mismatch between the two layers (See supplementary materials) would add a small correction to the measured spin-orbit splitting. Using Eq. 1 and the fitted effective masses, we obtain a value of 26.4 meV for spin-orbit coupling based on the measurement.

[27] Liu, G.-B., Xiao, D., Yao, Y., Xu, X. & Yao, W. Electronic structures and theoretical modelling of two-dimensional group-VIB transition metal dichalcogenides. *Chem. Soc. Rev.* **44**, 2643–2663 (2015).

[28] Rasmussen, F. A. & Thygesen, K. S. Computational 2d Materials Database: Electronic Structure of Transition-Metal Dichalcogenides and Oxides. *J. Phys. Chem. C* **119**, 13169–

13183 (2015).

[29] Latini, S., Winther, K. T., Olsen, T. & Thygesen, K. S. Interlayer Excitons and Band Alignment in MoS2/hBN/WSe2 van der Waals Heterostructures. *Nano Lett.* **17**, 938–945 (2017).

[30] Chaves, A., Azadani, J. G., zelik, V. O., Grassi, R. & Low, T. Electrical control of excitons in van der Waals heterostructures with type-II band alignment. *Physical Review B* **98** (2018).

[31] Previous measurements on bilayers with such commensurate twist angles showed instead interlayer excitons formed in the second Brillouin zone of the monolayer lattice, which have greatly reduced spectral weight compared to those in the first Brillouin zone in angularly-aligned bilayers [17].

[32] Xu, W. *et al.* Correlated fluorescence blinking in two-dimensional semiconductor heterostructures. *Nature* **541**, 62–67 (2017).

[33] Unuchek, D. *et al.* Room-temperature electrical control of exciton flux in a van der Waals heterostructure. *Nature* **560**, 340–344 (2018).

[34] Wang, G. *et al. Colloquium* : Excitons in atomically thin transition metal dichalcogenides. *Reviews of Modern Physics* **90** (2018).

[35] Tang, Y. *et al.* Simulation of Hubbard model physics in WSe2/WS2 moiré superlattices. *Nature* **579**, 353–358 (2020).

[36] Regan, E. C. *et al.* Mott and generalized Wigner crystal states in WSe2/WS2 moiré superlattices. *Nature* **579**, 359–363 (2020).

[37] Shimazaki, Y. *et al.* Strongly correlated electrons and hybrid excitons in a moiré heterostructure. *Nature* **580**, 472–477 (2020).

[38] Merkl, P. *et al.* Ultrafast transition between exciton phases in van der Waals heterostructures. *Nature Materials* **18**, 691–696 (2019).

[39] Wang, Z. *et al.* Evidence of high-temperature exciton condensation in two-dimensional atomic double layers. *Nature* **574**, 76–80 (2019).

[40] Zhang, X. *et al.* Gate-tunable spin waves in antiferromagnetic atomic bilayers. *arXiv:2001.04044 [cond-mat]* (2020).

[41] Karni, O. *et al.* Infrared Interlayer Exciton Emission in MoS_2/WSe_2 Heterostructures. *Physical Review Letters* **123**, 247402 (2019).

[42] Scuri, G. *et al.* Electrically tunable valley dynamics in twisted WSe2/WSe2 bilayers. *arXiv:1912.11306 [cond-mat]* 31 (2019).

[43] Tang, Y. *et al.* Spatially mixed moir excitons in two-dimensional van der waals superlattices. *arXiv:2002.10067 [cond-mat]* (2020). ArXiv:2002.10067.

[44] Bai, Y. *et al.* One-dimensional moiré excitons in transition-metal dichalcogenide heterobilayers. *arXiv:1912.06628 [cond-mat]* (2020). ArXiv:1912.06628.

[45] Jauregui, L. A. *et al.* Electrical control of interlayer exciton dynamics in atomically thin heterostructures. *Science* **366**, 870–875 (2019).

[46] Huang, Z. *et al.* Robust Room Temperature Valley Hall Effect of Interlayer Excitons. *Nano Letters* **20**, 1345–1351 (2020).

[47] Zhou, Y. *et al.* Controlling excitons in an atomically thin membrane with a mirror. *Phys. Rev. Lett.* **124**, 027401 (2020).

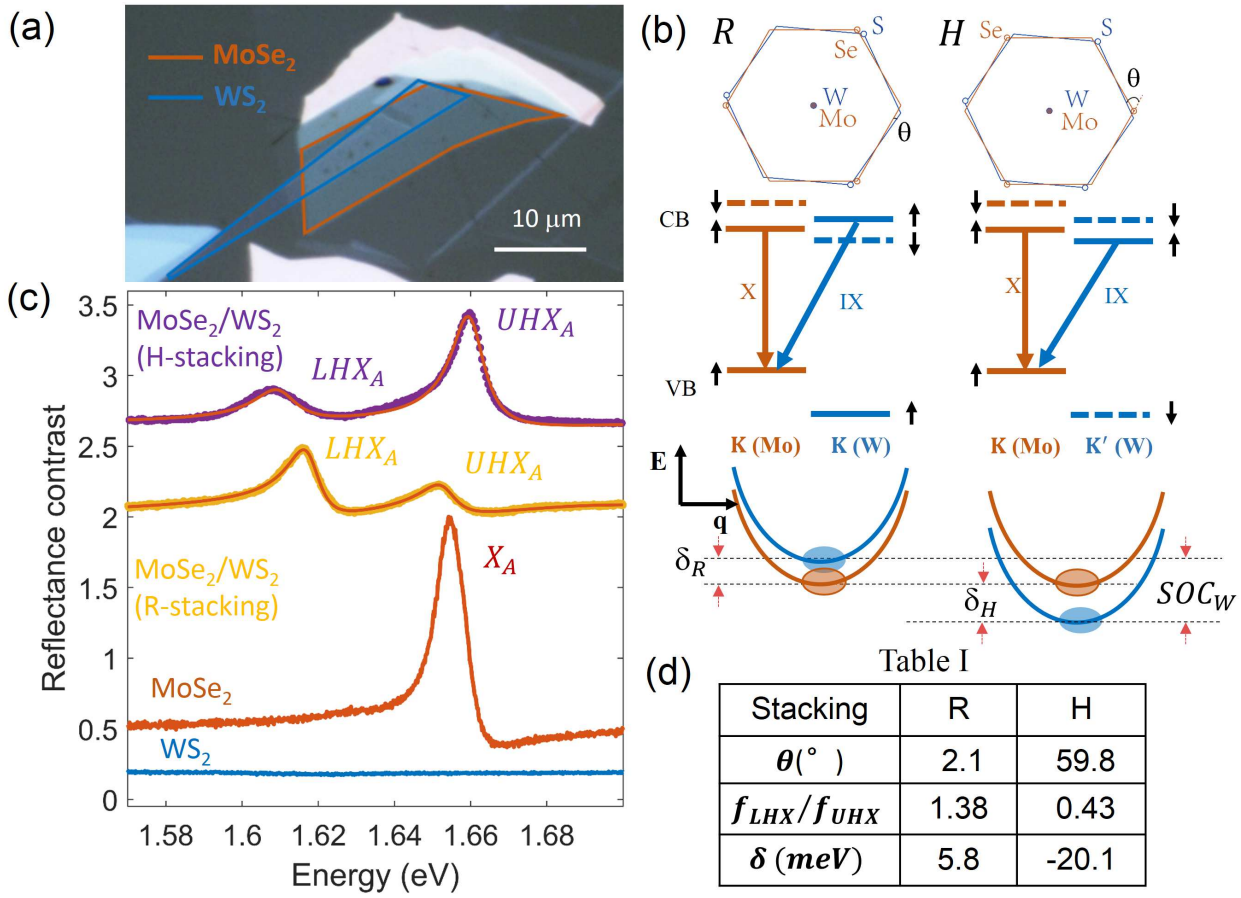

Stacking	R	H
$\boldsymbol{\theta}(^\circ)$	2.1	59.8
$\boldsymbol{f_{LHX}/f_{UHX}}$	1.38	0.43
$\boldsymbol{\delta}$ $\boldsymbol{(meV)}$	5.8	-20.1

FIG. 1: Hybrid excitons in rotationally aligned WS_2 /$MoSe_2$ bilayers. (a) Optical microscope image of an hBN-capped heterobilayer. Red and blue solid lines outline the $MoSe_2$ and WS_2 monolayers, respectively. (b) Top panels illustrate a unit cell of R-stacking (left) and H-stacking (right) WS_2 /$MoSe_2$ bilayers. Middle panels depict the corresponding band alignment of WS_2 and $MoSe_2$, where X labels the intra-layer transition and IX labels the nearly-resonant inter-layer transition that shares the same hole state. Solid and dashed lines corresponds to states of opposite spins. Bottom panels illustrate the alignment between an intra-layer $MoSe_2$ A exciton state (red) and the inter-layer exciton state (blue) that it hybridizes with. (c) Reflectance contrast (RC) spectra for, from bottom to top, a monolayer WS_2 (blue), monolayer $MoSe_2$ (red), R-stacking bilayer (orange) and H-stacking bilayer (purple). The dots are data and solid lines are fits. The spectra are displaced vertically for easier reading.(d) Summary of the fitted ratio of the oscillator strength between LHX and UHX, and the corresponding detuning δ .

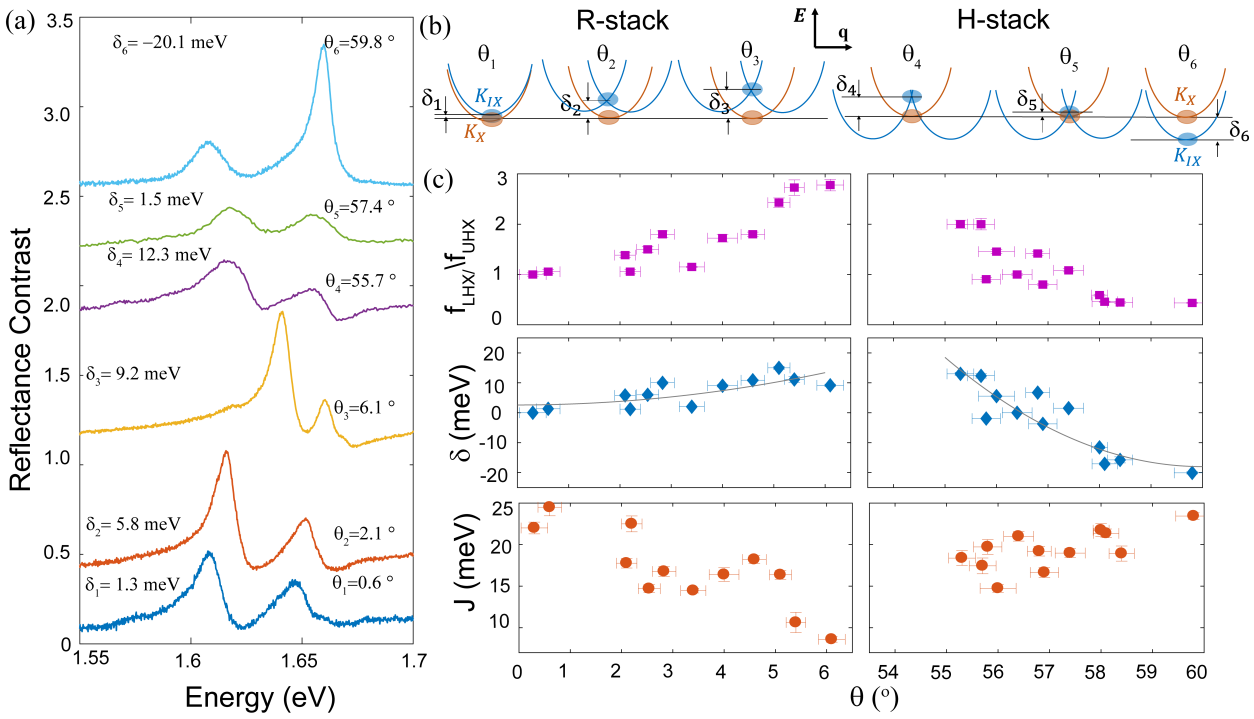

FIG. 2: Twist angle dependence of the hybrid excitons. (a) RC spectra of bilayers of different twist angles θ_i, for $i = 1$ to 6. The corresponding θ_i and extracted detuning $\delta_i = E_{IX,i} - E_{X,i}$ are labeled by each spectrum. The spectra are displaced vertically for easier reading (b) Schematics of MoA intra-layer (red) and inter-layer (blue) exciton bands at the different twist angles θ_i. The interlayer exciton band is displaced in the momentum space with increasing θ_i. The moiré superlattice leads to band folding and formation of a new interlayer exciton state at the Γ point $q = 0$ (blue oval), with the same angular momentum as the intralayer exciton state (red oval). (c) Ratio of the oscillator strengths of LHX_{MoA} and UHX_{MoA}, detuning, and inter- and intra-layer exciton coupling strength as a function of the twist angle θ, obtained from the RC spectra. The gray solid lines in the middle panel are quadratic fits based on equation 1.

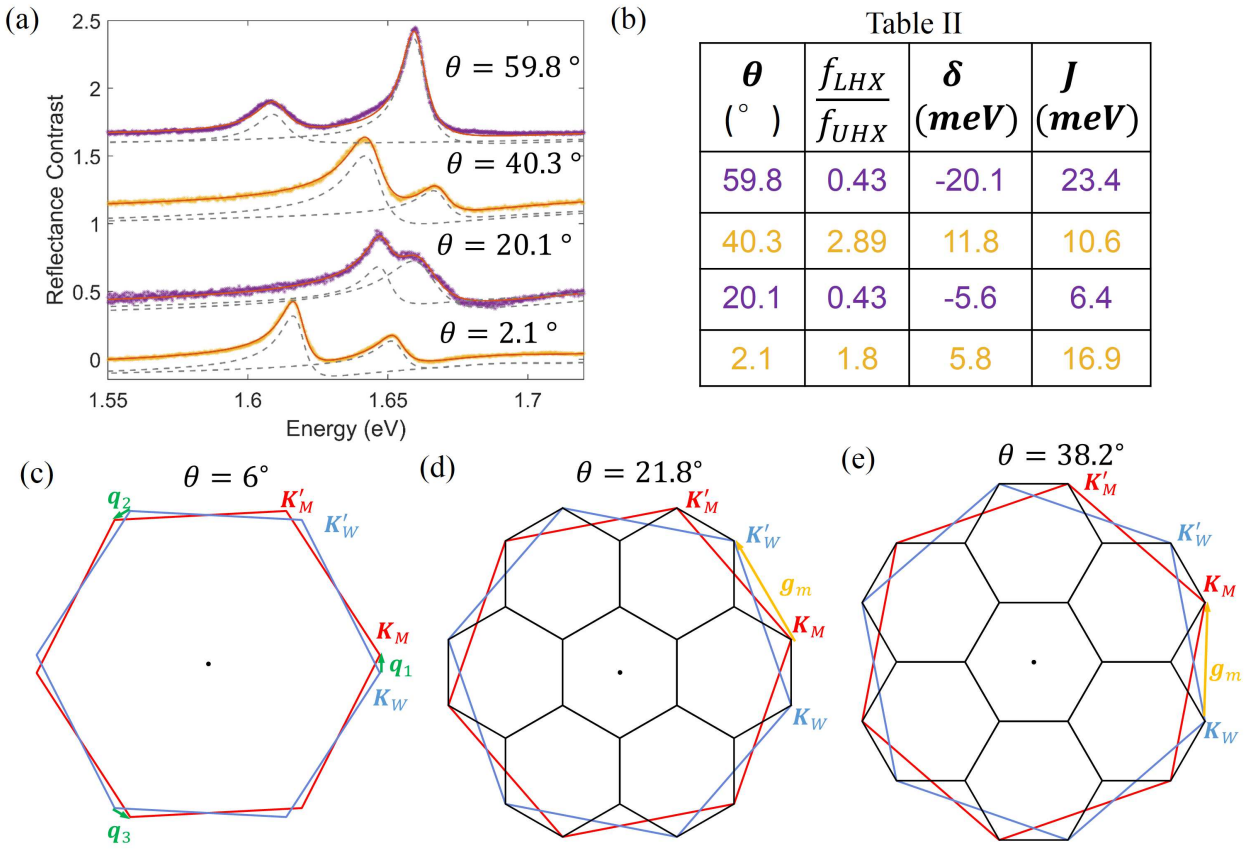

$\boldsymbol{\theta}$ (°)	$\frac{f_{LHX}}{f_{UHX}}$	$\boldsymbol{\delta}$ (meV)	$\boldsymbol{J}$ (meV)
59.8	0.43	-20.1	23.4
40.3	2.89	11.8	10.6
20.1	0.43	-5.6	6.4
2.1	1.8	5.8	16.9

FIG. 3: Hybridization in commensurate moiré lattices compared with aligned bilayers. (a) RC spectra of bilayers with $\theta = 2.1°, 20.1°, 40.3°$ and $59.8°$. The LHX has a higher (lower) spectral weight than UHX in bilayers with $\theta = 2.1°$ and $40.3°$ ($\theta = 59.8°$ and $20.1°$). Dots are data, solid lines are fits, and dashed lines are the fitted individual hybrid exciton resonances. (b) Summary of the fitted parameters for the RC spectra in a, showing similarities between bilayers with $\theta = 2.1°$ and $40.3°$ and between bilayers with $\theta = 59.8°$ and $20.1°$. (c-e) Schematics of the Brillouin zones of twisted bilayers. The red (blue) hexagons depict the Brillouin zones of $MoSe_2$ (WS_2) monolayers. In (c), the twist angle is $6°$. The green arrows indicate vectors $\boldsymbol{q}_1$, $\boldsymbol{q}_2$ and $\boldsymbol{q}_3$, which represent the momentum shift between the Brillouin zone corners of the two monolayers. In (d), $\theta = 21.8°$, a commensurate moiré lattice is formed, with the corresponding moiré Brillouin zone depicted by the black hexagons. The yellow arrow represents the moiré reciprocal lattice base vector that connects $\boldsymbol{K}_M$ and $\boldsymbol{K}'_W$. In (e), $\theta = 38.2°$, which is another commensurate angle dual to $21.8°$, and $\boldsymbol{K}_M$ and $\boldsymbol{K}_W$ become equivalent states in the moiré Brillouin zone.

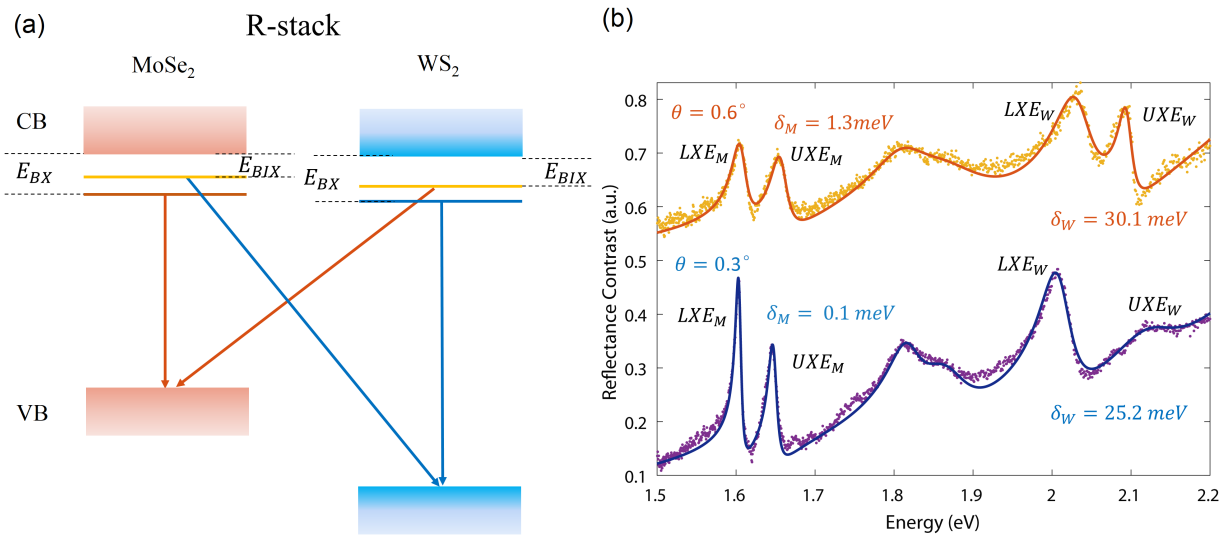

FIG. 4: Comparison of MoA and WA hybrid states. (a) Band diagram of R-stacking $MoSe_2$ /WS_2 bilayers. The conduction and valence bands are represented by broad continuous bands. Exciton states are represented by the horizontal solid lines. Arrows represent spin-conserved exciton transitions, which are lowered in energy from the band-to-band transition by a binding energy. E_{BX} and E_{BIX} denote the binding energies for the intra- and inter-layer transitions, respectively. (c) RC spectra of both MoA and WA hybrid excitons from bilayers with $\theta \sim 0°$. Dots are data and solid lines are fits. The corresponding θ and detuning δ_M and δ_W obtained from fitting are labeled by each spectrum.

Figures

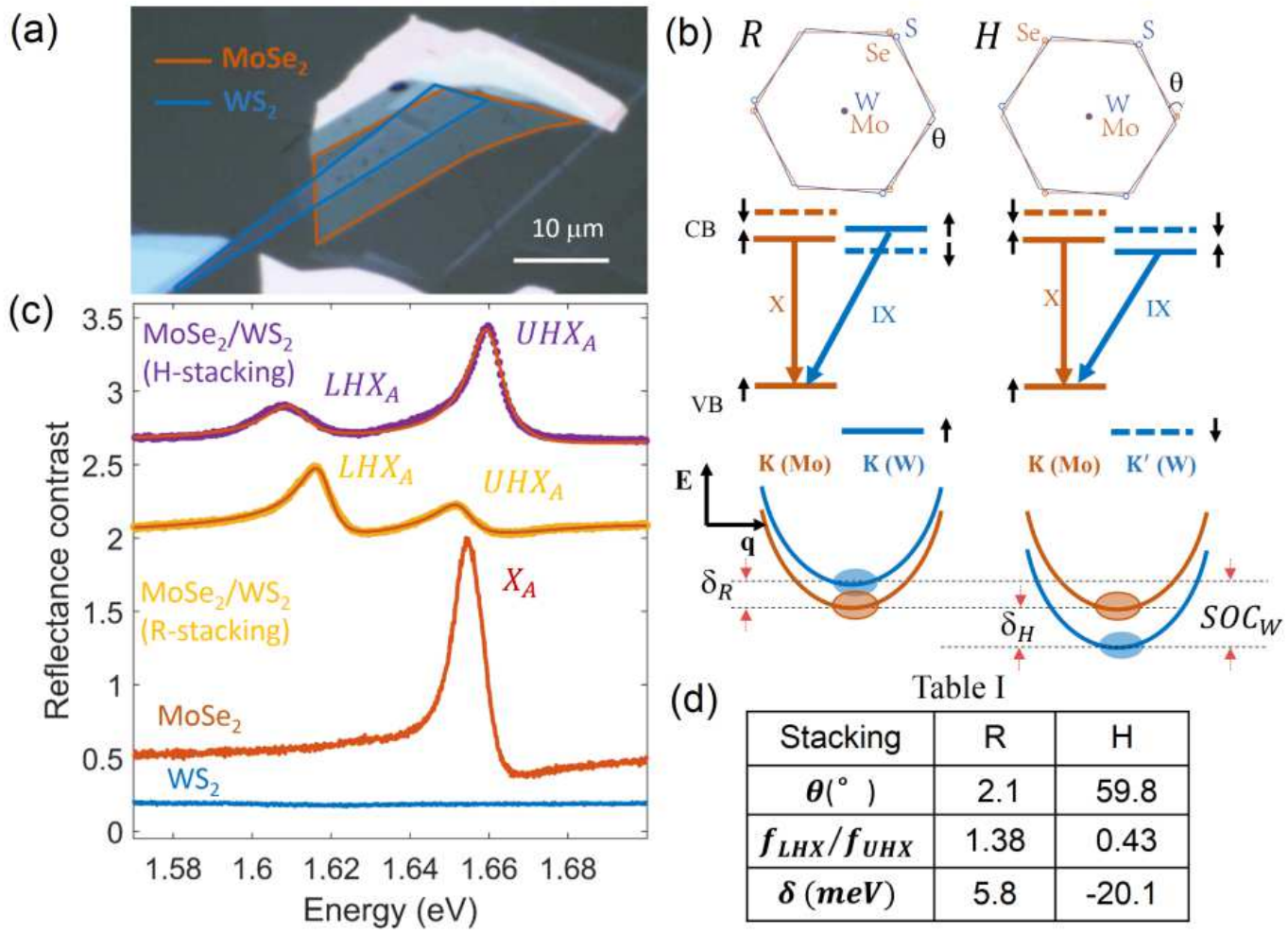

(d)

Table I

Stacking	R	H
$\boldsymbol{\theta}(^\circ)$	2.1	59.8
$\boldsymbol{f_{LHX}/f_{UHX}}$	1.38	0.43
$\boldsymbol{\delta\ (meV)}$	5.8	-20.1

Figure 1

Hybrid excitons in rotationally aligned WS2 /MoSe2 bilayers. (a) Optical microscope image of an hBN-capped heterobilayer. Red and blue solid lines outline the MoSe2 and WS2 monolayers, respectively. (b) Top panels illustrate a unit cell of R-stacking (left) and H-stacking (right) WS2 /MoSe2 bilayers. Middle panels depict the corresponding band alignment of WS2 and MoSe2 , where X labels the intra-layer transition and IX labels the nearly-resonant inter-layer transition that shares the same hole state. Solid and dashed lines corresponds to states of opposite spins. Bottom panels illustrate the alignment between an intra-layer MoSe2 A exciton state (red) and the inter-layer exciton state (blue) that it hybridizes with. (c) Reflectance contrast (RC) spectra for, from bottom to top, a monolayer WS2 (blue), monolayer MoSe2 (red), R-stacking bilayer (orange) and H-stacking bilayer (purple). The dots are data and solid lines are fits. The spectra are displaced vertically for easier reading.(d) Summary of the fitted ratio of the oscillator strength between LHX and UHX, and the corresponding detuning δ .

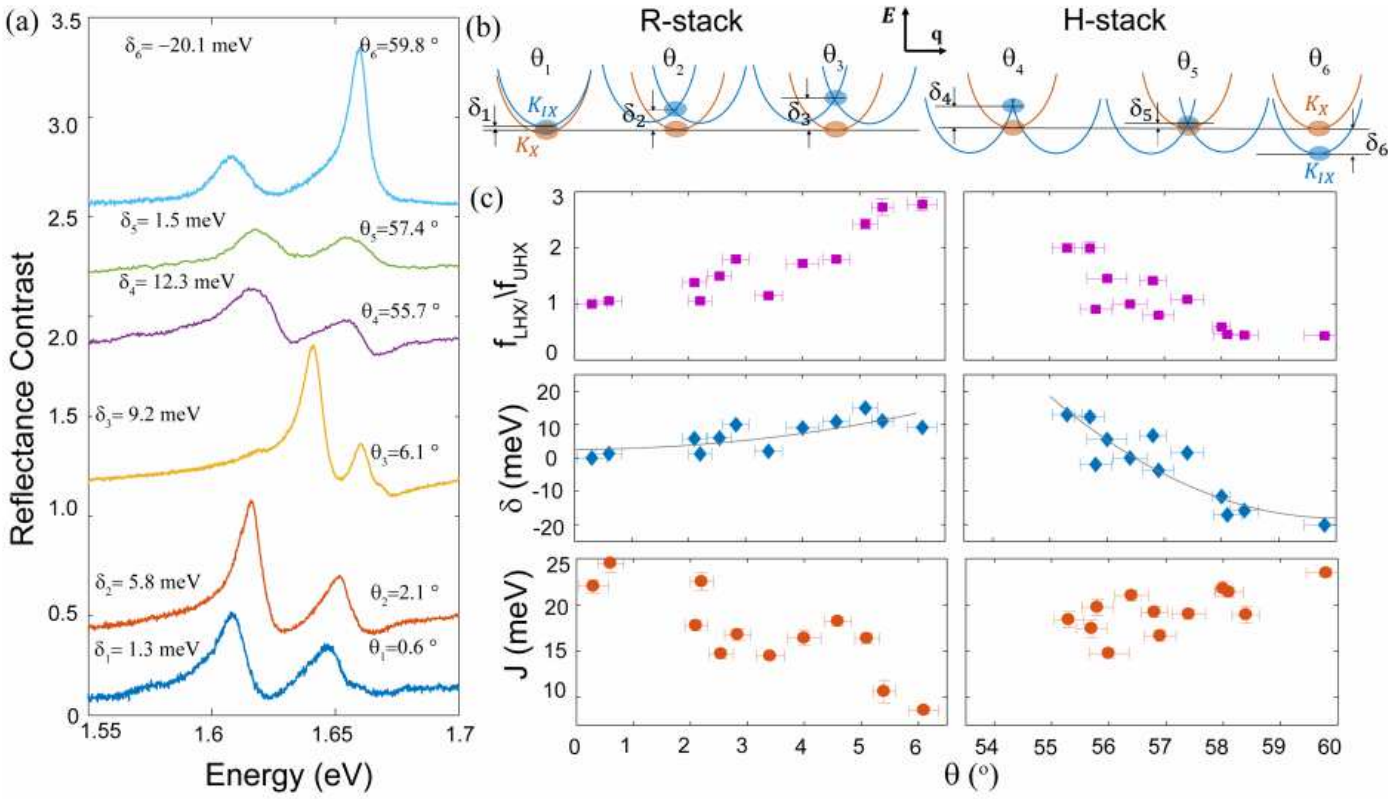

Figure 2

Twist angle dependence of the hybrid excitons. (a) RC spectra of bilayers of different twist angles θi , for i = 1 to 6. The corresponding θi and extracted detuning δi = EIX,i − EX,i are labeled by each spectrum. The spectra are displaced vertically for easier reading (b) Schematics of MoA intra-layer (red) and inter-layer (blue) exciton bands at the different twist angles θi . The interlayer exciton band is displaced in the momentum space with increasing θi . The moir´e superlattice leads to band folding and formation of a new interlayer exciton state at the Γ point q = 0 (blue oval), with the same angular momentum as the intralayer exciton state (red oval). (c) Ratio of the oscillator strengths of LHXM oA and UHXM oA, detuning, and inter- and intra-layer exciton coupling strength as a function of the twist angle θ, obtained from the RC spectra. The gray solid lines in the middle panel are quadratic fits based on equation 1.

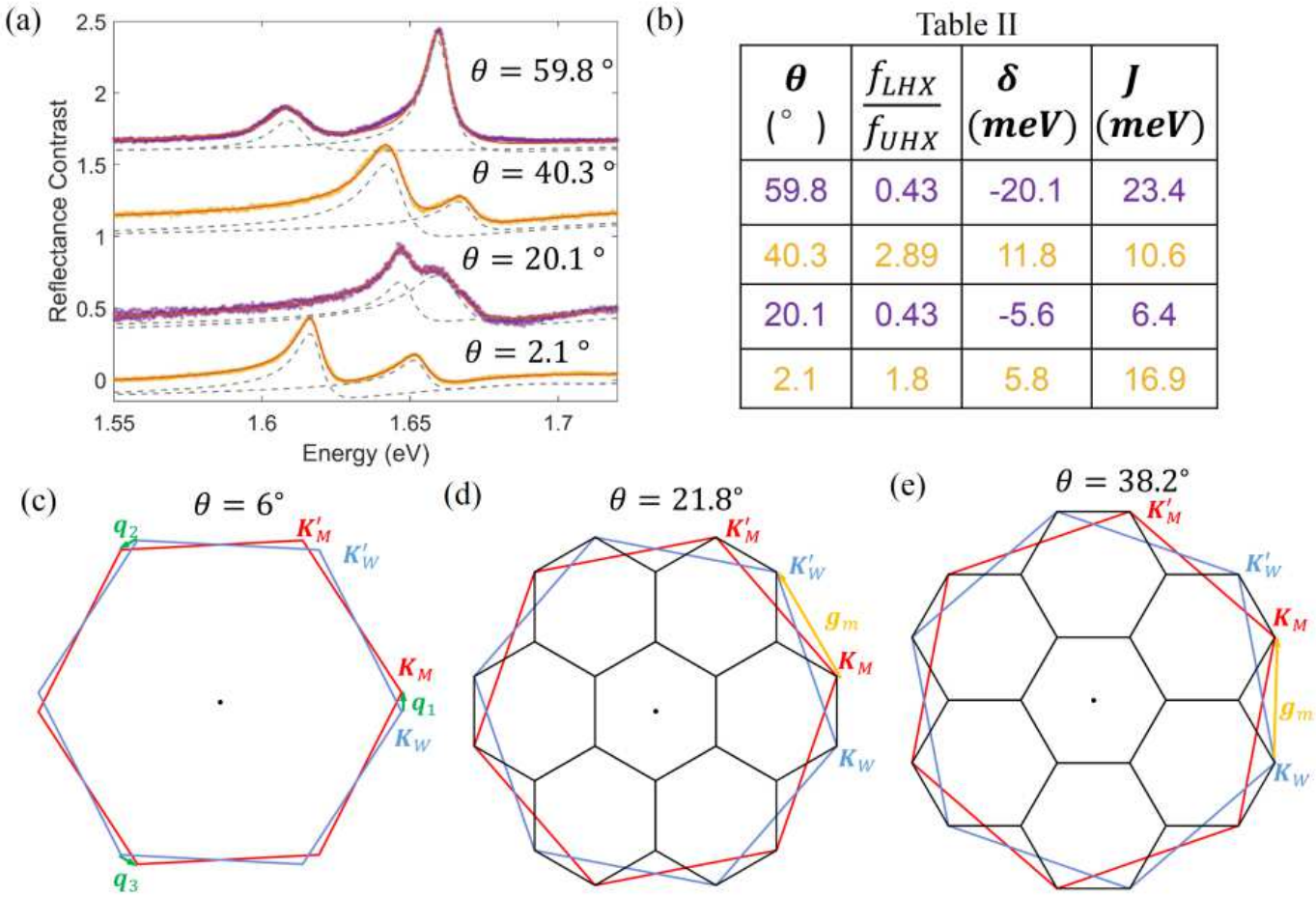

θ (°)	$\frac{f_{LHX}}{f_{UHX}}$	δ (meV)	J (meV)
59.8	0.43	-20.1	23.4
40.3	2.89	11.8	10.6
20.1	0.43	-5.6	6.4
2.1	1.8	5.8	16.9

Figure 3

Hybridization in commensurate moir´e lattices compared with aligned bilayers. (a) RC spectra of bilayers with θ = 2.1 ◻ , 20.1 ◻ , 40.3 ◻ and 59.8 ◻ . The LHX has a higher (lower) spectral weight than UHX in bilayers with θ = 2.1 ◻ and 40.3 ◻ (θ = 59.8 ◻ and 20.1 ◻). Dots are data, solid lines are fits, and dashed lines are the fitted individual hybrid exciton resonances. (b) Summary of the fitted parameters for the RC spectra in a, showing similarities between bilayers with θ = 2.1 ◻ and 40.3 ◻ and between bilayers with θ = 59.8 ◻ and 20.1 ◻ . (c-e) Schematics of the Brillouin zones of twisted bilayers. The red (blue) hexagons depict the Brillouin zones of MoSe2 (WS2) monolayers. In (c), the twist angle is 6 ◻ . The green arrows indicate vectors q1, q2 and q3, which represent the momentum shift between the Brillouin zone corners of the two monolayers. In (d), θ = 21.8 ◻ , a commensurate moir´e lattice is formed, with the corresponding moir´e Brillouin zone depicted by the black hexagons. The yellow arrow represents the moir´e reciprocal lattice base vector that connects KM and K0 W . In (e), θ = 38.2 ◻ , which is another commensurate angle dual to 21.8 ◻ , and KM and KW become equivalent states in the moir´e Brillouin zone.

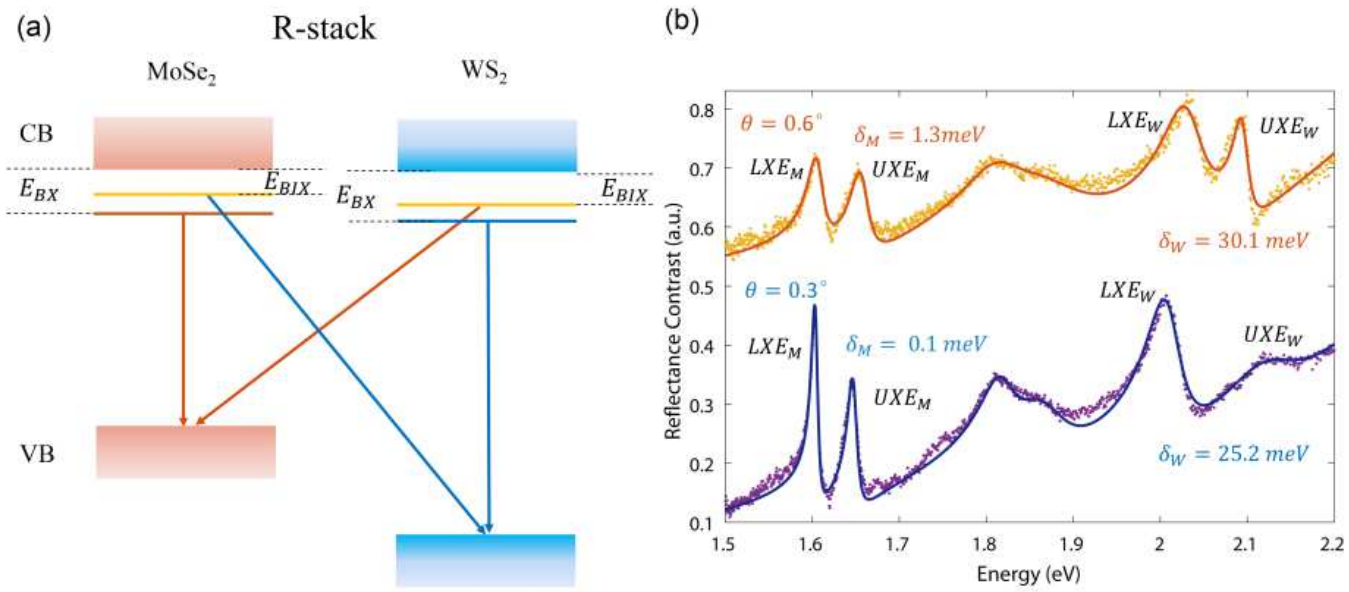

Figure 4

Comparison of MoA and W A hybrid states. (a) Band diagram of R-stacking MoSe2 /WS2 bilayers. The conduction and valence bands are represented by broad continuous bands. Exciton states are represented by the horizontal solid lines. Arrows represent spin-conserved exciton transitions, which are lowered in energy from the band-to-band transition by a binding energy. EBX and EBIX denote the binding energies for the intra- and inter-layer transitions, respectively. (c) RC spectra of both MoA and W A hybrid excitons from bilayers with θ ≈ 0 °. Dots are data and solid lines are fits. The corresponding θ and detuning δM and δW obtained from fitting are labeled by each spectrum.

Supplementary Files

This is a list of supplementary files associated with this preprint. Click to download.

- ZhangSupplementary.pdf